TU Delft

Delft University of Technology

Cyclic behavior of C-shaped masonry wall retrofitted with twisted bars or bonded rebars

Scamardo, M.; Cattaneo, S.; Crespi, P.; Vafa, N.

DOI
10.1016/j.conbuildmat.2024.137703

Publication date
2024

Document Version
Final published version

Published in
Construction and Building Materials

Citation (APA)
Scamardo, M., Cattaneo, S., Crespi, P., & Vafa, N. (2024). Cyclic behavior of C-shaped masonry wall retrofitted with twisted bars or bonded rebars. *Construction and Building Materials*, *443*, Article 137703. https://doi.org/10.1016/j.conbuildmat.2024.137703

Important note
To cite this publication, please use the final published version (if applicable).
Please check the document version above.

Copyright
Other than for strictly personal use, it is not permitted to download, forward or distribute the text or part of it, without the consent of the author(s) and/or copyright holder(s), unless the work is under an open content license such as Creative Commons.

Takedown policy
Please contact us and provide details if you believe this document breaches copyrights.
We will remove access to the work immediately and investigate your claim.

This work is downloaded from Delft University of Technology.
For technical reasons the number of authors shown on this cover page is limited to a maximum of 10.

Construction and Building Materials 443 (2024) 137703

Contents lists available at ScienceDirect

Construction and Building Materials

journal homepage: www.elsevier.com/locate/conbuildmat

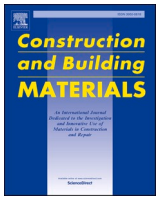

Cyclic behavior of C-shaped masonry wall retrofitted with twisted bars or bonded rebars

M. Scamardo [a,*], S. Cattaneo [a], P. Crespi [a], N. Vafa [b]

[a] ABC Dept., Politecnico di Milano, Milan, Italy
[b] Faculty of Civil Engineering and Geosciences, Delft University of Technology, Delft, the Netherlands

ARTICLE INFO

Keywords:
Masonry retrofitting
Cyclic loading
Bonded fastener
Twisted bars
Full-scale testing
Wall to wall connections

ABSTRACT

The lack of effective connection between masonry walls is one of the most common reasons leading to the activation of out-of-plane failure mechanisms in masonry buildings during earthquakes. Thus, retrofitting interventions aimed at improving the box-like behavior of masonry structures are of primary importance. The paper presents the results of an experimental program aimed at investigating the effectiveness of two different fastening solutions to improve the joint connection of masonry walls in existing unreinforced masonry buildings. A full scale C-shaped clay brick masonry specimen was built featuring purposely weakened wall intersections. Vertical prestress was applied on top of the specimen to represent the weights of upper floors. The specimen was first tested in the unreinforced configuration under monotonic out-of-plane displacement, until a main crack was detected. Then, its corner connections were repaired using twisted bars, and tested under cyclic out-of-plane displacement. Lastly, the twisted bars were removed and replaced with bonded bars, and the specimen was tested again under cyclic out-of-plane displacement. The test results showed that both retrofitting solutions were able to recover the full capacity of the unreinforced wall, with higher displacement and dissipation capacity for the twisted bars solution, and higher resistance for bonded bars. The latter seems to be the most effective solution, especially in terms of monolithic behavior achieved; however, the large displacements associated to twisted bars could be a great advantage in case of earthquake actions.

1. Introduction

Unreinforced masonry (URM) buildings usually exhibit severe damage and collapse after strong earthquake events [1–4]. This high vulnerability with respect to horizontal loads is mainly due to the brittle behavior and low tensile strength of the material, considering also that most of URM buildings were built before the introduction of seismic design codes, taking into account only gravity loads.

Retrofitting techniques have become more and more important for the upgrading of the existing building stock. In the design of the interventions, a more comprehensive approach should be considered aimed at improving not only the structural safety, but also the comfort and energy savings [5].

The earthquake response of URM buildings strongly depends on the execution and detailing of the walls. If effective connections among the different structural elements are guaranteed and the so-called box-like behavior is achieved [6], the horizontal actions can be properly distributed over the bearing walls. In this case, out-of-plane failures are prevented, the building acts as a jointly assemblage of walls and floors, and a global response of the structure is expected. If the box-like behavior is not achieved, the walls of the building behave independently, and local failure mechanisms can be activated, with potential loss of stability of parts of the structure [7,8].

Several retrofitting techniques have been developed by researchers and engineers, using traditional or innovative materials, with the aim of improving the seismic resistance of URM buildings and achieving a box-like behavior [9–11]. In particular, strengthening systems aimed at improving the connections between bearing walls are essential to avoid out-of-plane mechanisms.

Metal ties with end bars or plates have been used for this scope since long time (e.g., in Italy from the 15th century) [12]. They contribute to guarantee an efficient connection between walls, also playing an important role in the control of horizontal thrusts in vaults and arches. Their use has the advantage to be low-invasive, reversible and low-expensive, but the devices remain visible and require a high maintenance cost over time due to the corrosion phenomena usually

* Corresponding author.
E-mail address: manuela.scamardo@polimi.it (M. Scamardo).

https://doi.org/10.1016/j.conbuildmat.2024.137703
Received 14 April 2024; Received in revised form 10 June 2024; Accepted 30 July 2024
Available online 2 August 2024
0950-0618/© 2024 The Authors. Published by Elsevier Ltd. This is an open access article under the CC BY license (http://creativecommons.org/licenses/by/4.0/).

affecting steel elements. As an alternative to metal ties, fiber-reinforced polymer (FRP) ties have been more recently proposed [13] with the advantage of having a higher durability and chemical inertia against corrosion phenomena with respect to steel, and reduced weight.

Another common methodology to improve the connection between masonry elements is the use of post-installed fasteners. They usually consist of injected anchors made of steel or fiber reinforced polymers bars installed with cement/lime grout or adhesive into pre-drilled boreholes crossing the orthogonal walls [14–19]. These solutions offer a very good level of connection between the elements, a low invasiveness and an easy applicability. On the other side, depending on the type of bars and grout adopted, corrosion phenomena (for steel bars) and pulverization of the grouts may occur over time.

As alternative, a new type of connector made of twisted stainless-steel bars [20–24] has been recently proposed, which can also be installed "dry" without any adhesive by using a special mandrel to screw-in the bar in the pre-drilled hole. Twisted bars are commonly used for crack stitching [25], reinforced repointing or near surface mounted insertion [26–28]. However, their application for the strengthening of masonry connections seems promising [29], especially in historical buildings where compatibility, durability and removability requirements must be satisfied [30,31]. The main drawback of this approach is the high cost.

Despite the widespread use of post-installed fasteners to improve masonry connections, it is surprising that only limited scientific literature is available on the topic [14], either in terms of experimental research or design approaches. In particular, testing of connections is rarely performed on full scale specimens. Paganoni et al. [18] tested a T-shaped masonry wall made with recycled hand-cut solid bricks, in which the connections were improved using post-installed grouted stainless-steel anchors. Maddaloni et al. [19] tested a full-scale T-shaped tuff masonry wall, with grouted anchors made by hollow CFRP pultruded carbon tubes to improve the connection. No references are instead available, to the authors knowledge, on the use of twisted bars (installed "dry") as connectors (with the exception of the work already presented by the authors in [29]).

Design codes [32–34] underline the importance to include effective connections in the seismic retrofit of masonry buildings, but a lack of specific design rules is evident, often requiring engineers to design such interventions on the basis of qualitative approaches.

With the aim of giving a contribution for the characterization of strengthening systems used for the improvement of masonry connections and to address the technical gaps described above, an experimental program has been conducted on full scale masonry specimens, considering two different retrofitting solutions: a "dry" screw-type connection realized with twisted stainless-steel bars, and a bonded fasteners connection using steel rebars. The use of rebars represents the most common and cheap solution. However, in case of historical heritage buildings, reversibility and compatibility must also be considered [30,31]. In this regard, twisted bars have the advantage of being removable without causing significant damage on the base material. Furthermore, the durability of stainless steel is also a great benefit, allowing to overcome typical problems of corrosion due to the use of steel bars, while the "dry" application avoids any chemical compatibility issue that can arise with the use of hybrid adhesives [29].

This paper presents the results of experiments conducted on a full-scale C-shaped masonry wall made of clay bricks. An analogous study on a full-scale T-shaped wall has been previously presented by the authors [25]. The perpendicular connections of the specimen walls were designed to represent typical weak connections, often observed in existing URM buildings. To achieve this scope, the classical English bond rule was locally modified by reducing the number of interlocking bricks. The specimen was subjected to out-of-plane horizontal displacement to simulate the out-of-plane actions due to earthquakes. The specimen was tested in the as-built unreinforced configuration, and in the repaired configurations, considering the two different types of connectors mentioned above. Three subsequent test runs were performed on the masonry specimen: (i) a monotonic test on the unreinforced configuration, (ii) a cyclic test on the twisted bars retrofitted configuration, (iii) a cyclic test on the retrofitted configuration with bonded bars, installed after the removal of twisted bars. During the tests, a vertical prestress was applied to simulate the common gravity loads acting on the walls of masonry buildings. The main experimental evidence and findings are presented and discussed in the following.

2. Experimental program

2.1. Geometry and materials

The geometry of the masonry specimen is depicted in Fig. 1. The total height of the wall was 2.11 m, the front wall length 2.20 m, and the side walls length 1.62 m. The thickness of both front and back walls was 25 cm.

Solid clay bricks "Rosso vivo" (250×120×55 mm) and M2.5 cementitious mortar were used to build a double-whyte specimen assembled in English bond, which is very widespread in Italy. The mechanical properties of the bricks were characterized by means of compressive and splitting tests, executed according to [35] and [36], respectively. The mean compressive strength, evaluated perpendicularly to the bed surface of the brick on six bricks, resulted in 23.3 MPa, with a coefficient of variation of 5.5 %. The mean tensile (splitting) strength, evaluated on three bricks, resulted in 2.5 MPa, with a coefficient of variation of 18.3 %. To assess the mechanical properties of the mortar, 18 samples were taken at different stages of construction of the specimen. All samples were aged more than 28 days and then, compressive, three-point bending, and splitting tests were conducted according to [37–39]. The mean compressive, bending, and splitting strengths of the mortar resulted 4.6 MPa, 2.0 MPa and 0.6 MPa, respectively.

The interlocking between the wall panels was designed in a weak way to simulate adverse in-situ conditions often observed in existing masonry constructions. The aim was to trigger failure at the joint section between the front and back walls. The weakening of the connection was achieved by locally modifying the standard English bond rule (A-C-A-C, Fig. 1) with the introduction of "weak" courses without any brick interlocking along the height of the wall (layer B, Fig. 1). The B-layers replaced 3 out of 4 C-layers. The resulting spacing between the interlocking C-layers was chosen according to Italian common practice for cases where a new wall is erected between two existing ones (i.e., around 50 cm). Indeed, in such cases, usually some bricks are removed and replaced to bridge the old and the new walls (blue bricks of layer C in Fig. 1).

2.2. Retrofitting with twisted bars

Twisted stainless-steel bars (AISI 304) [20] were used to strengthen the unreinforced specimen (Fig. 2a). The bar had a nominal diameter of 12 mm, a nominal cross section area of 15.1 mm^2 and a total length of 100 cm. The nominal yielding and ultimate loads declared by the producer were 16.1 kN and 18.9 kN, respectively, and the elastic modulus was higher than 122 GPa. The bars layout at each corner is reported in Fig. 2b. The total embedment depth in the wall varied depending on the position/orientation of the bar from 50 to 80 cm. The twisted bars were installed at mid-height of the bricks. A sketch of the front wall with the twisted bars positions and quantities is shown in Fig. 3a. A total of 42 bars were installed to connect the front and the rear walls: 8 twisted bars at 60° (blue), 8 twisted bars at 30° (red), and 5 twisted bars at 90° (pink) were used on each corner. Assuming adjacent buildings on either side and to avoid installation from the (hypothetical) inside of the building, all bars were installed from the front side. Additionally, 20 twisted bars at 45° (Fig. 2c) were used to stitch the bending cracks that appeared on the front wall after the first monotonic loading test of the unreinforced specimen.

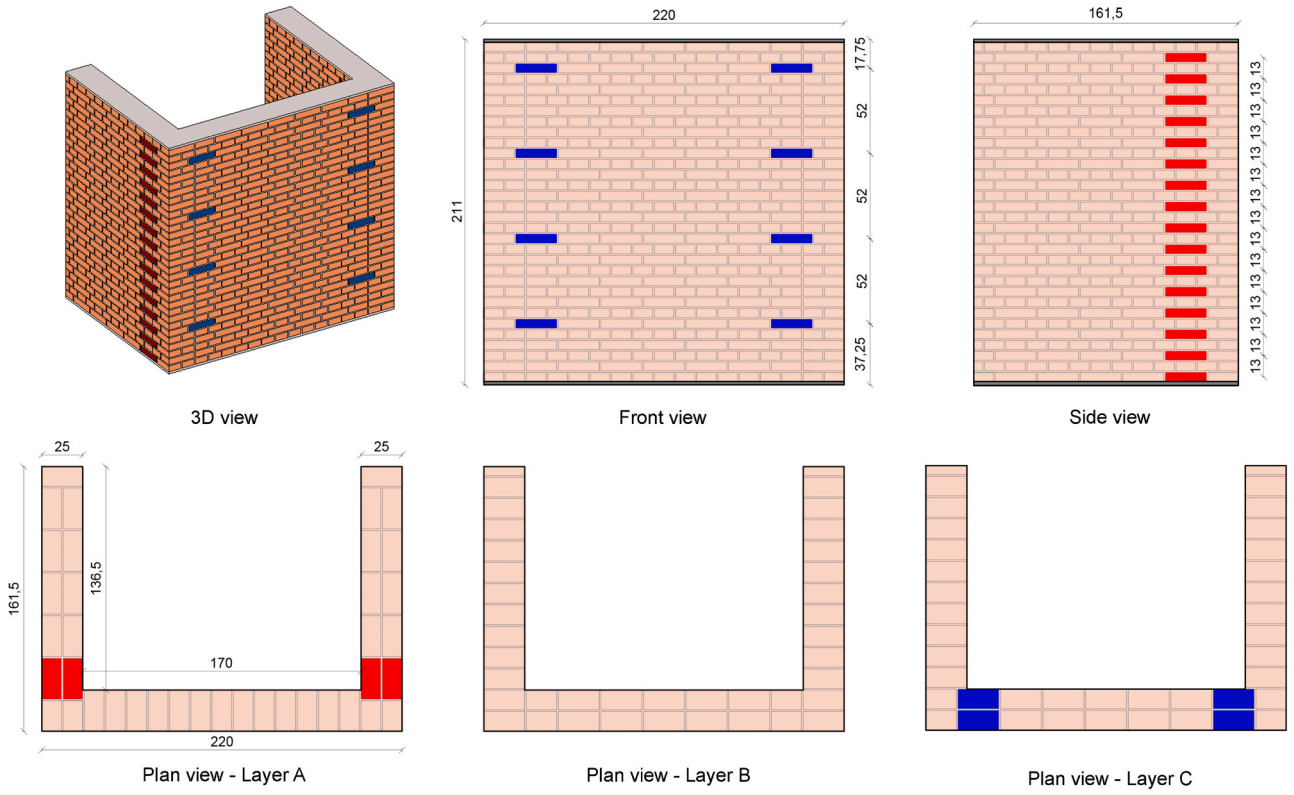

Fig. 1. Geometry of the specimen (measures in cm).

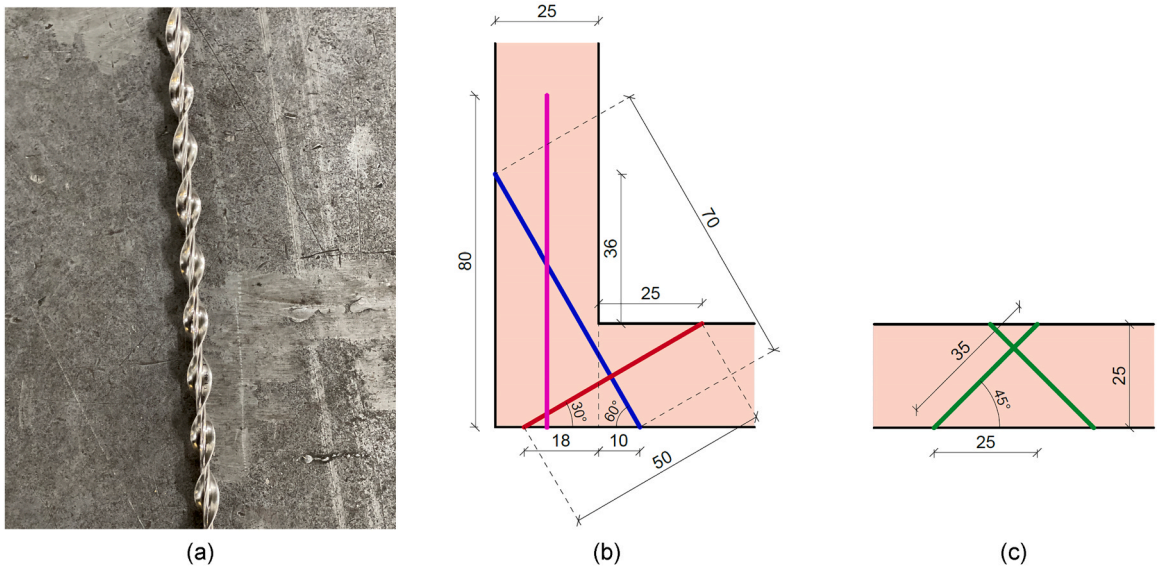

Fig. 2. Twisted bar (a), installation lay-out at the corner (b) and on the front wall for the crack stitching (c) (measures in cm).

The twisted bars were installed according to the following steps. After defining and marking the position of the bars on the wall, the holes were realized by using a drilling machine equipped with a drill bit of 8 mm nominal diameter (Fig. 4a). Holes were drilled to a longer depth (10 cm more than required) to avoid any issue related to the accumulation of masonry debris at the tip of the hole during the bar installation. Each hole was then cleaned by compressed air for at least three times (Fig. 4b). Finally, twisted bars were installed by using a hammer drilling machine equipped with a special hammering device supplied by the manufacturer (Fig. 4c). Fig. 5a shows the specimen retrofitted with the twisted bars.

2.3. Retrofitting with post-installed rebars and injection mortar

After testing the wall specimen retrofitted with twisted bars, the latter were pulled-out with a hydraulic jack (Fig. 4d) and replaced by a reduced number of 12 mm diameter steel rebars (B450C) installed with injection mortar (Fig. 4e-f). Thereby, the pre-existing hole diameter was enlarged from 8 mm to 14 mm by using a hammer drilling machine to enable the installation of the rebars with injection mortar. In this way,

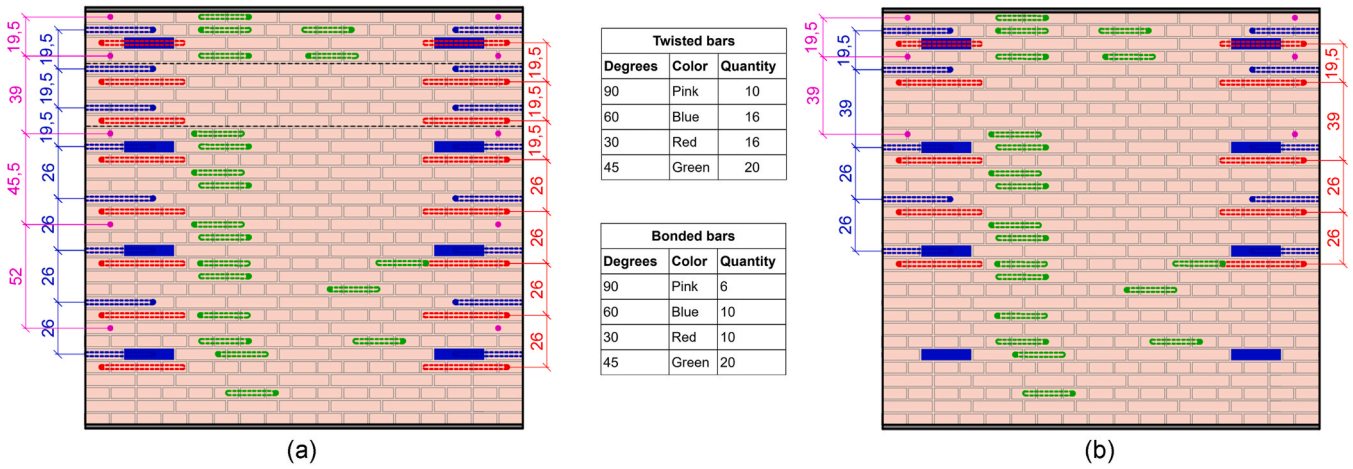

Twisted bars		
Degrees	Color	Quantity
90	Pink	10
60	Blue	16
30	Red	16
45	Green	20

Bonded bars		
Degrees	Color	Quantity
90	Pink	6
60	Blue	10
30	Red	10
45	Green	20

Fig. 3. Position and quantities of twisted bars (a) and bonded bars (b) (measures in cm).

Fig. 4. Retrofitting steps: (a) hole drilling, (b) compressed air cleaning, (c) twisted bar installation, (d) twisted bar removal, (e) adhesive injection, (f) rebar installation.

also the damaged masonry substrate caused by the previous test phase was removed. The injection anchoring system Hilti HIT-HY 270 [40] for applications in brick masonry was adopted as adhesive. Each hole was cleaned by compressed air for at least two times, then a steel brush was used two times from front to back, and again the compressed air was blown into the hole two additional times.

Fig. 5. Specimen retrofitted with twisted bars (a) and bonded bars (b).

A sketch of the wall with the rebars positions and quantities is shown in Fig. 3b. The total number of bars to reinforce the corner connections was reduced from 42 (twisted bars configuration) to 26 due to the higher pull-out strength of the rebars with respect to the twisted bars [22,41]. In particular, 5 rebars at 60° (blue), 5 rebars at 30° (red), and 3 rebars at 90° (pink) were used on each corner. The same embedment depths of twisted bars were considered (Fig. 2b). 20 additional rebars at 45° (green) with 35 cm of embedment depth replacing all twisted bars were used to stitch the bending cracks that appeared on the front wall. Fig. 5b shows the specimen retrofitted with the bonded steel rebars.

2.4. Test setup

The horizontal load was applied with a hydraulic actuator with capacity of 300 kN, equipped with an AEP TC4 load cell (Fig. 6). The point of application of the load was situated at 167 cm from the floor. This measure was selected to maximize the lever arm of the horizontal load with respect to the ground and to fit the reaction frame of the laboratory, given the height of the specimen (211 cm). A horizontal steel beam was placed on the front wall (Fig. 7a) and connected to the hydraulic jack to distribute the point load along the whole width of the front wall. On the opposite side of the front wall, another steel beam (Fig. 7b) was placed and connected to the loading beam by means of threaded rods, in order to transfer the horizontal load to the whole specimen. The system of steel beams allowed the proper distribution of the applied load, avoiding the formation of local damages close to the application point of the horizontal force.

Four additional jacks were used to apply a vertical prestress of

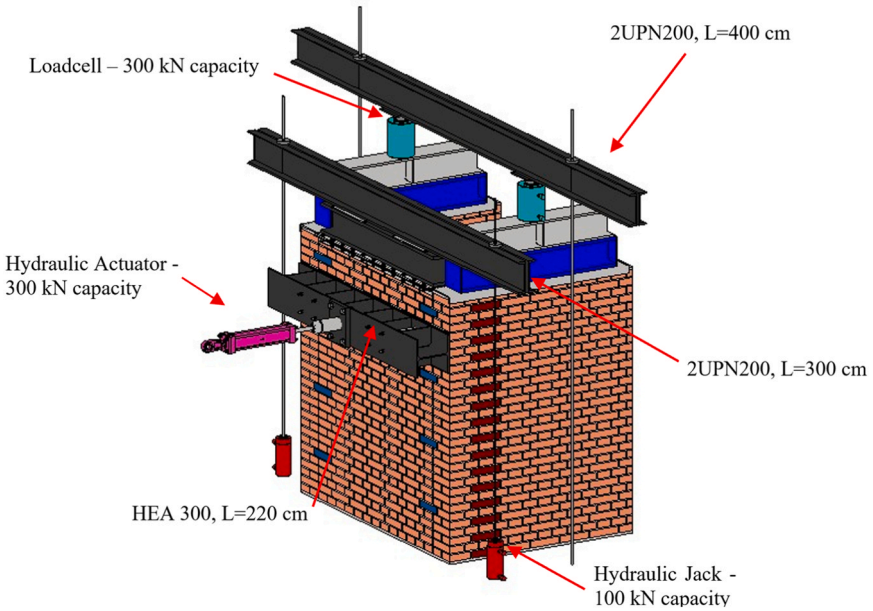

Fig. 6. Test set-up.

Fig. 7. Front view (a) and back view (b) of the specimen with the test set-up.

0.2 MPa on the walls, associated to the service loads: two jacks were applied on the front wall, and one on each back wall. A system of steel beams, connected to the strong floor by threaded bars, was used to distribute the load on top of the walls (Fig. 6). The vertical load was measured using four load cells in series with the jacks. The load was kept (almost) constant during the execution of the tests by controlling the pressure in the jacks. Exceptionally, the prestress was increased up to 0.25 MPa in the last part of the cyclic test with bonded bars in the attempt of reducing the uplift observed on the back walls. It should be noted that, along with the rocking of the specimen, the prestress loading system develops a horizontal stabilizing component. However, considering the limited amount of horizontal drift, this load was not taken into account.

To monitor the displacements and crack opening fields observed during the tests, 27 linear variable differential transformers (LVDTs) were placed on the specimen (Fig. 8). Each LVDT has an identification code that includes the type of measure and the position (in cm) with respect to the bottom of the specimen. In particular, the transducers can be grouped into the following main categories: (i) absolute displacement of the front wall on the left side (FL), in the middle (FM), and on the right side (FR); (ii) relative displacement between the back and the front wall on the left side (BL) and on the right side (BR); (iii) absolute horizontal displacement at the top of the rear walls on the left (BHL) and right (BHR) side; (iv) absolute vertical displacement at the top of the rear walls on the left (BVL) and right (BVR) side; (v) absolute lateral horizontal displacement at top of the front wall on the left (FHL) and right (FHR) side; (vi) measure of the vertical deformation of the front wall during the preliminary monotonic test on the left side (FVL), on the right side (FVR), and on the back in the middle (BVM); (vii) crack width opening on the front wall measured only during cyclic tests at the top (CRFT) and bottom (CRFB) of the front wall.

2.5. Test program and loading protocol

To assess the different retrofitting solutions (i.e. twisted bars and bonded bars), the investigation was subdivided in different phases. Before starting the test, a vertical prestress of about 0.2 MPa was applied to the walls and kept constant throughout all the tests (unless mentioned otherwise).

First, a monotonic test was performed on the unreinforced wall by applying a horizontal out-of-plane displacement until the first major event (FME) was detected. The FME is usually associated to the formation of the first crack. The increasing displacement was applied at a rate of 0.05 mm/s. Once the FME was reached, the wall was unloaded.

Secondly, the damaged specimen was repaired using twisted bars, installed according to the configuration of Fig. 3a, and a cyclic test was

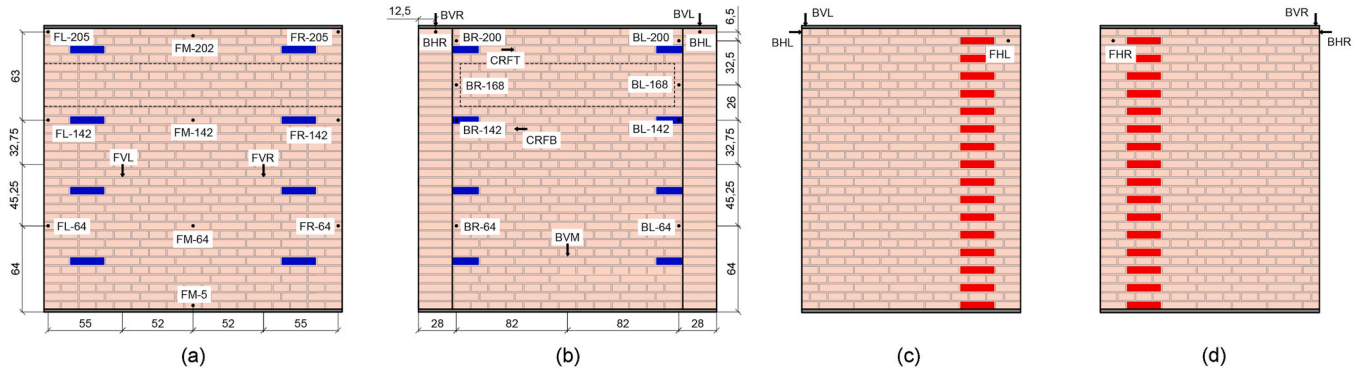

Fig. 8. LVDTs position on the wall: (a) front view, (b) back view, (c) left view, (d) right view (measure in cm).

performed. The theoretical displacement protocol is reported in Fig. 9. Starting from the zero horizontal displacement of the monotonic test, the displacement amplitude was progressively increased in steps of 25 % of the FME displacement, performing three repeated cycles for each displacement level. The test was stopped when the damage/safety condition of the specimen became risky, and the horizontal jack unloaded. Then, the twisted bars were removed using a hydraulic jack, avoiding any possible damage of the surrounding masonry.

Finally, twisted bars were replaced by bonded bars installed according to the configuration of Fig. 3b, and another cyclic test was performed with the same protocol previously adopted for the twisted bars retrofitting solution.

It should be highlighted that, while performing the cyclic tests, a residual displacement was evident already at the first cycles due to the development of damage in the specimen. For this reason, during the unloading phase, it was not possible to go back to zero displacement and the cycles were ended when the horizontal load was null (otherwise, compression should have been applied on the front wall).

3. Test results

3.1. Monotonic test on unreinforced specimen

The results of the test on the unreinforced specimen under monotonic horizontal displacement in terms of load vs stroke (at the horizontal jack level) and load vs time are reported in Fig. 10, respectively. Fig. 10b reports also the vertical prestress loads measured on the front (green curve) and back (red curve) walls (right vertical axis). The first observed damage, associated to the FME, was a vertical crack situated in the middle of the front wall (Fig. 11, left). It was detected at a load of 82.0 kN and a displacement (stroke) of 7.9 mm. Right after, a sudden drop of the horizontal load to 72.3 kN was observed. The damage suggested a bending failure of the front wall due to the out-of-plane loading. With further increase of the imposed displacement, two additional cracks appeared along the vertical connecting joints plus another vertical crack on the external side of the left back wall (Fig. 11, right). At this point, the test was stopped, and the specimen unloaded (zero horizontal load).

The maximum load reached during the test was 86.9 kN, associated to a stroke of 11.2 mm (drift ratio 0.67 %). The horizontal displacement reached the maximum value of 13.4 mm, and a residual displacement of 6.4 mm was measured at the end of the test. The prestress loads had a limited variation during the test and ranged between 80.2 kN (0.19 MPa) and 85.3 kN (0.20 MPa) on the front wall, and between 158.5 kN (0.20 MPa) and 163.7 kN (0.20 MPa) on the back walls.

Fig. 12 shows the load-displacement curves of the transducers placed on the front wall, considering the absolute values (a), the relative displacements between front and back walls (b), and a comparison between them (c). As expected, looking at the absolute displacements (FM, FL, FR), higher values were measured on the top (solid curves), while decreasing displacements were detected towards the bottom of the specimen. Moreover, higher displacements in the middle of the front wall (green curves) with respect to the lateral ones were also evident, confirming the bending of the front wall (Fig. 12a). The relative displacements between the front and back walls (BL, BR) were negligible until cracking occurred. In particular, on the right side (Fig. 13a), a major crack crossing the front wall was evident in the area at the top of the steel beam (BR-200), while the other right transducers did not record any significant displacement. On the left side (Fig. 13b), the observed crack involved a larger area crossing the back wall, and displacements were recorded also below the steel beam. Fig. 12c shows the comparison between the absolute displacements at the top of the front (FL-205 and FR-205) and back (BHL and BHR) walls. The "B" transducers have been changed in sign for better comparison. The displacements almost overlapped up to the peak load on the left side, and up to the end of the test on the right side. The difference between absolute and relative displacements observed on the left side was due to the crack opening along the side of the left wall after the peak load (Fig. 13b). The crack width recorded reached 2.89 mm.

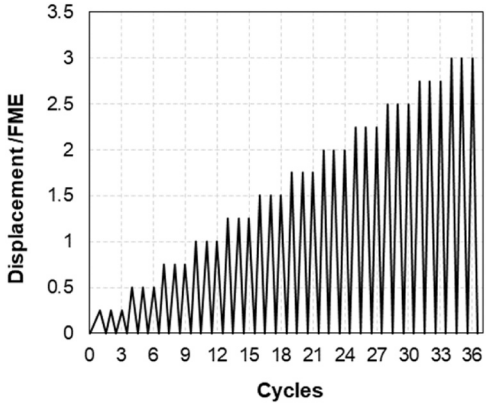

Fig. 9. Cyclic test loading protocol.

3.2. Cyclic loading with twisted bars

After the monotonic test phase, the specimen was retrofitted with twisted bars to improve the corner connection between front and back walls as described in Section 2.2. The specimen was subjected to a cyclic test with increasing horizontal displacement steps according to Section 2.5 and the protocol reported in Fig. 9. The displacement recorded during the monotonic test and associated to the FME (7.5 mm) was used as reference. The residual displacement obtained at the end of the monotonic test (6.72 mm) was neglected by setting the initial horizontal displacement to zero at the beginning of the cyclic test.

Overall, 33 cycles were performed up to 275 % of the FME displacement. The test was stopped when the value of the load was essentially stable and a noticeable out-of-plane displacement of the front wall was observed.

Fig. 14 shows the results of the test in terms of the imposed displacement vs time (a), load vs time (b) and load vs displacement at the horizontal jack level (c). As above, Fig. 14b also reports the vertical prestress load measured on the front and back walls (right vertical axis). The maximum load reached during the test was 89.7 kN, associated to a stroke of 20.6 mm (drift ratio 1.23 %). In each group of cycles, a slight degradation of the load over the cycles was evident, with a load drop ranging between the 3.0 % and 4.2 % for the second cycle, and between the 4.0 % and 7.4 % for the third cycle. Fig. 14a and Fig. 14c show a residual displacement associated to the development of damage in the specimen. The residual displacement increases with the increase of the imposed displacement, suggesting a significant dissipation capacity of the system.

The prestress loads had a limited variation during the test and ranged between 80.7 kN (0.19 MPa) and 85.3 kN (0.20 MPa) on the front wall, and between 159.4 kN (0.20 MPa) and 166.6 kN (0.21 MPa) on the back walls (Fig. 14b). It should be highlighted that, while the loads recorded by the two cells on the front wall were similar, a difference was detected on the back walls between the left and right load cell, with a higher load on the right one (84.7 kN vs 81.9 kN). This difference may be attributed to the fact that an uplift of the right back wall was recorded, which was not observed on the left side, probably because of the vertical crack formed during the monotonic test (Fig. 11b) that weakened the connection between the left back wall and the front wall.

Fig. 15 shows the crack pattern on the front wall at the end of the cyclic test with twisted bars, in which a bending crack is evident in the middle (as in the monotonic test) and vertical detachment cracks are visible in the connecting joints.

Looking at the load vs displacement curves reported in Fig. 16 and

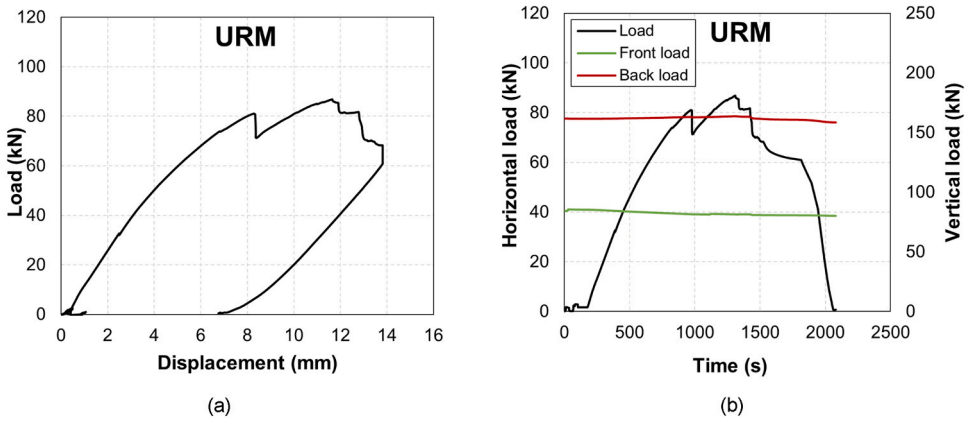

Fig. 10. Load-displacement (a) and load-time (b) curves of the unreinforced monotonic test.

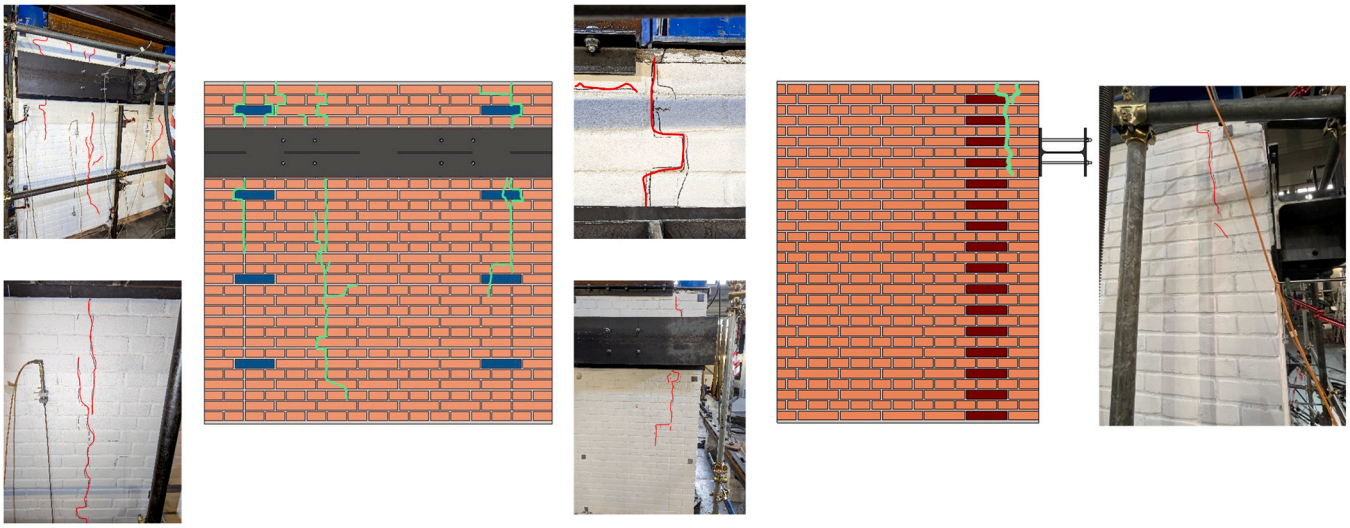

Fig. 11. Crack details after FME of URM specimen: front view (left), and left side view (right).

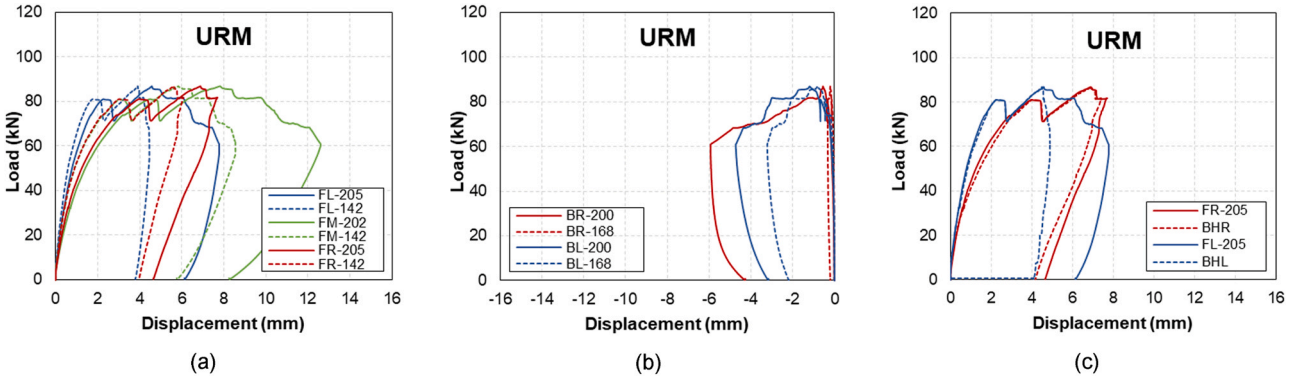

Fig. 12. Load-displacement curves of front wall transducers: (a) absolute displacement, (b) relative displacement between front and back walls, (c) comparison between absolute and relative displacement at the top of the wall.

obtained from the LVDTs located on the front wall, a larger displacement is evident going from the bottom to the top. The displacements result higher (maximum of 19.63 mm) also in the middle with respect to the sides, confirming the horizontal bending detected during the monotonic test. Moreover, the left side of the wall shows higher displacements (max. 10.59 mm) with respect to the right side (max. 7.11 mm), which is an effect of the pre-existing crack on the side of the left back wall. A progressive residual displacement was also measured by all transducers, especially the ones located at the top of the wall (11.03 mm).

Fig. 17 shows the relative displacements measured between the front and back walls on the left and right side (Fig. 17a and Fig. 17b, respectively), and the vertical displacement, i.e. uplift, measured on the back walls (Fig. 17c). A significant detachment of the back right wall from the front wall is evident, especially at the top (13.21 mm on BR-

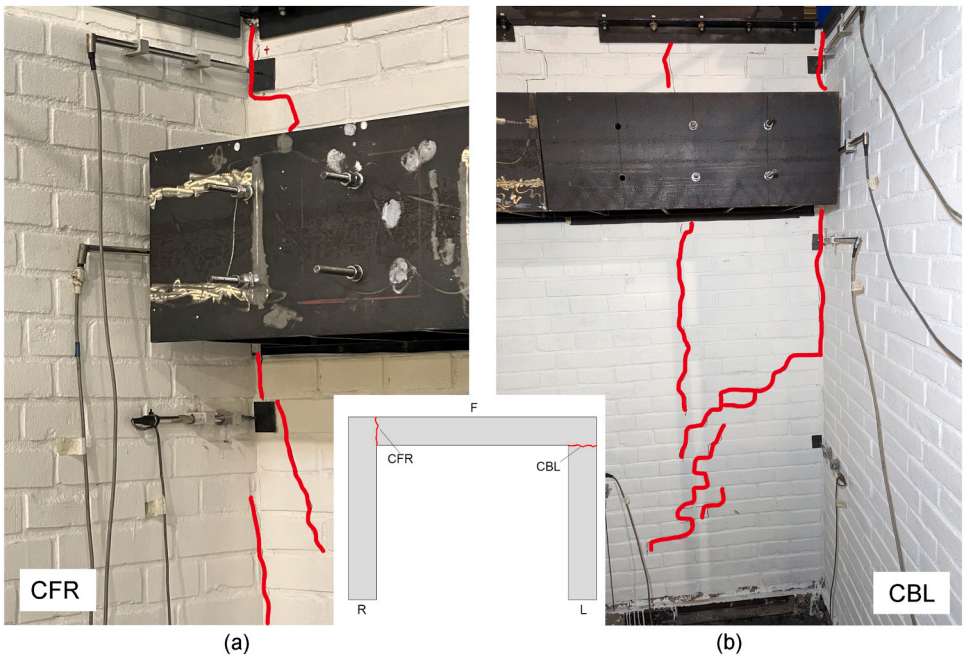

Fig. 13. Cracking observed after the monotonic test: (a) back view, right side; (b) back view, left side.

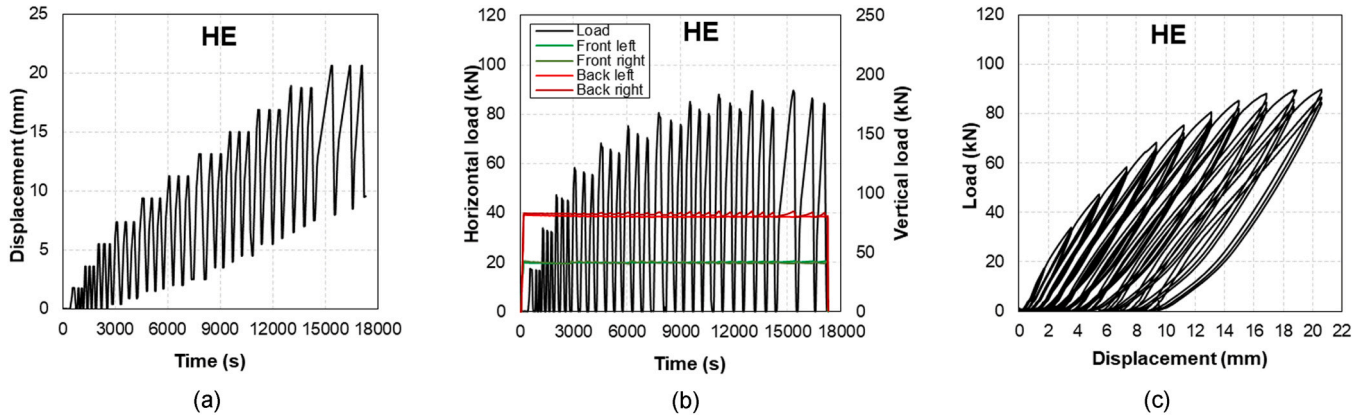

Fig. 14. (a) Horizontal (stroke) displacement-time, (b) load-time and (c) load-displacement (stroke) curves of the cyclic test with twisted bars.

200), while at lower levels the LVDTs showed limited displacement. On the left wall, the maximum displacement was lower (8.71 mm on BL-200) with respect to the right wall, but the detachment was observed also at lower levels. However, despite the observed detachment/cracks, the twisted bars were able to well connect the walls, as proved by the uplift recorded (Fig. 17c), especially on the right wall.

After this test phase, the twisted bars were removed to prepare the specimen for the follow-up installation of the rebars with adhesive.

3.3. Cyclic loading with rebars and adhesive

After removing the twisted bars, a total of 26 rebars with HY270 adhesive were installed according to the layout presented in Section 2.3. The loading protocol replicated the one adopted for the cyclic test with twisted rebars (Fig. 9). However, after the cycle at 175 % of FME, a quite constant value of the horizontal load (about 100 kN) was detected, despite the increasing imposed displacement. In fact, a rigid motion of the whole specimen was observed, while a constant prestress load was maintained. At this point, the vertical prestress was increased from 0.2 to 0.25 MPa to investigate the effect of this parameter on the overall behavior of the specimen. It should be noticed that, to maintain the vertical prestress constant on the back walls, it was necessary to increase the pressure in the back jacks during the unloading phases, and reduce it during the loading phases.

Overall, 27 cycles were performed up to 225 % of the FME displacement. The test was finally stopped when the overturning of the specimen was activated.

Fig. 18 shows the results of the test in terms of the imposed displacement vs time (a), load vs time (b) and load vs displacement (c). As before, Fig. 18b reports also the vertical prestress load measured on the front and back walls (right vertical axis). The maximum horizontal load reached during the test was 114.8 kN, associated to a stroke of 16.9 mm (drift ratio 1.01 %), and to a vertical prestress on the back wall 0.25 MPa. The maximum load associated to the prestress of 0.2 MPa was 100.9 kN.

A limited residual displacement is evident from Fig. 18a and Fig. 18c, which slightly increases with the increase of the imposed displacement, suggesting a limited dissipation capacity of the system. The variation of the vertical load on the front wall was limited, ranging from 79.71 kN (0.19 MPa) to 84.46 kN (0.20 MPa) in the first part of the test, and from 97.84 kN (0.23 MPa) to 170.84 kN (0.25 MPa) when the prestress load was increased. The vertical load on the back walls had greater variation

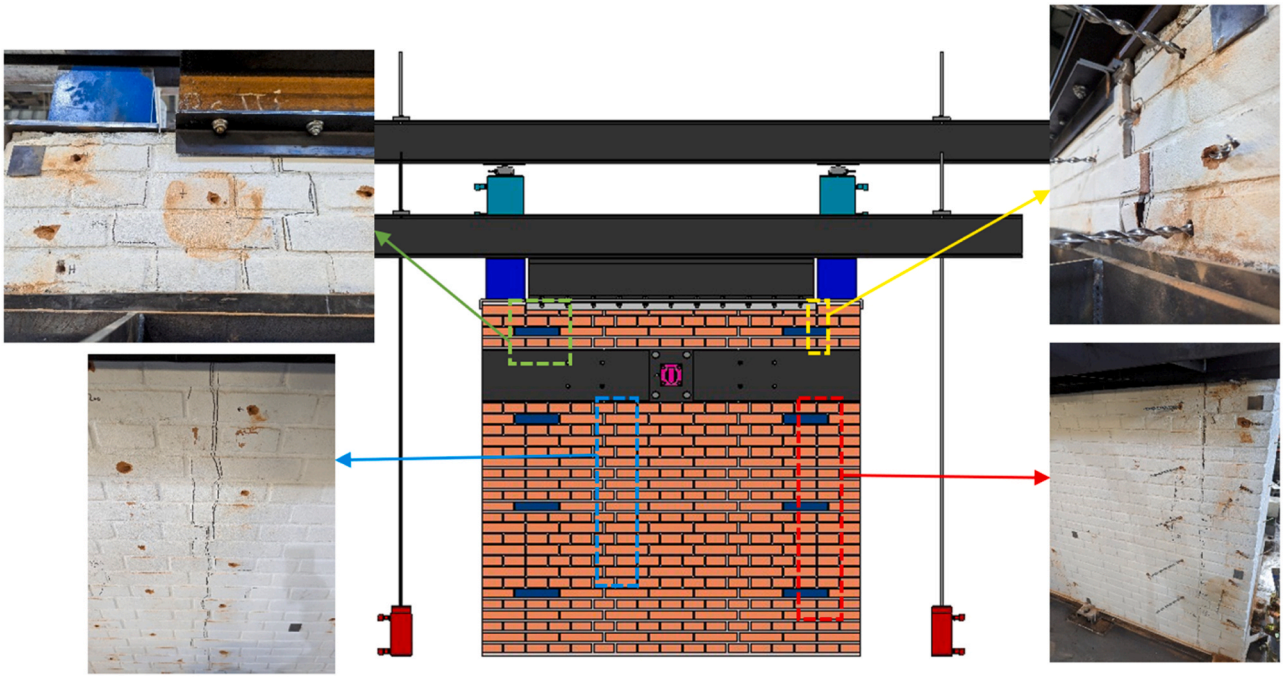

Fig. 15. Crack pattern at the end of the test with twisted bars – front side.

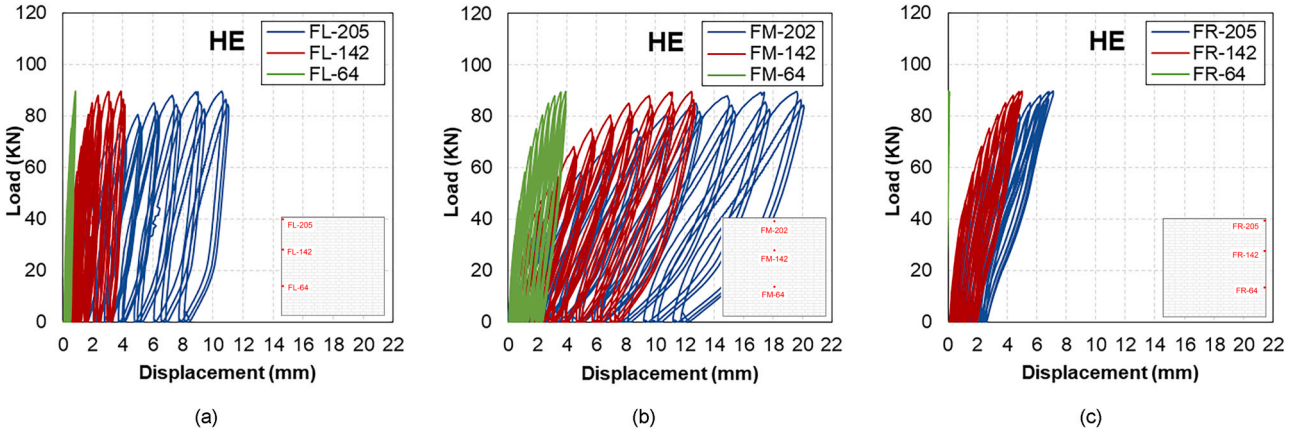

Fig. 16. Load-displacement (LVDT) curves at different height of the front wall: (a) left side, (b) middle, (c) right side.

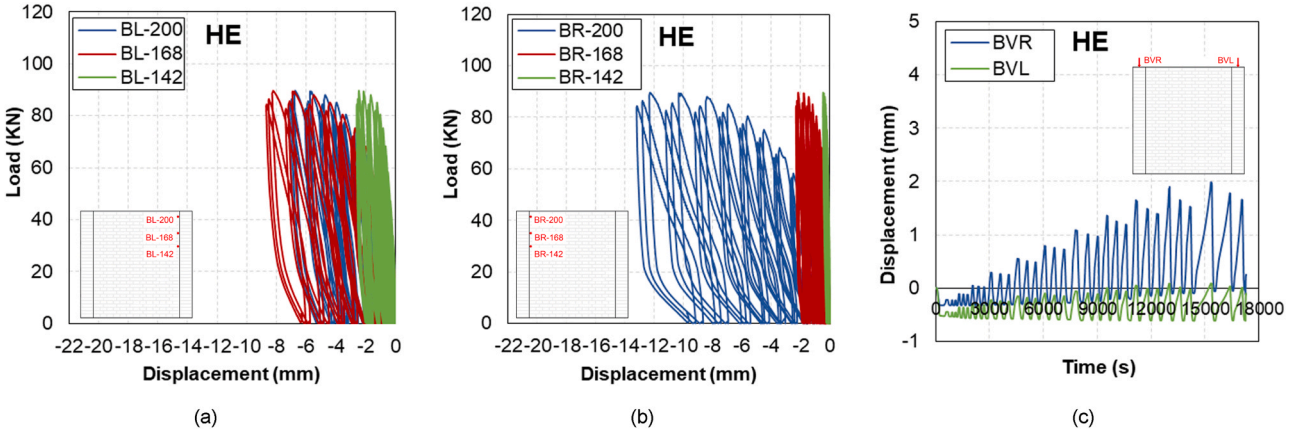

Fig. 17. Load-displacement (LVDT) curves at different height of the front wall measured from the back: (a) relative displacement on left side and (b) relative displacement on right side. In (c), vertical displacement on the back walls.

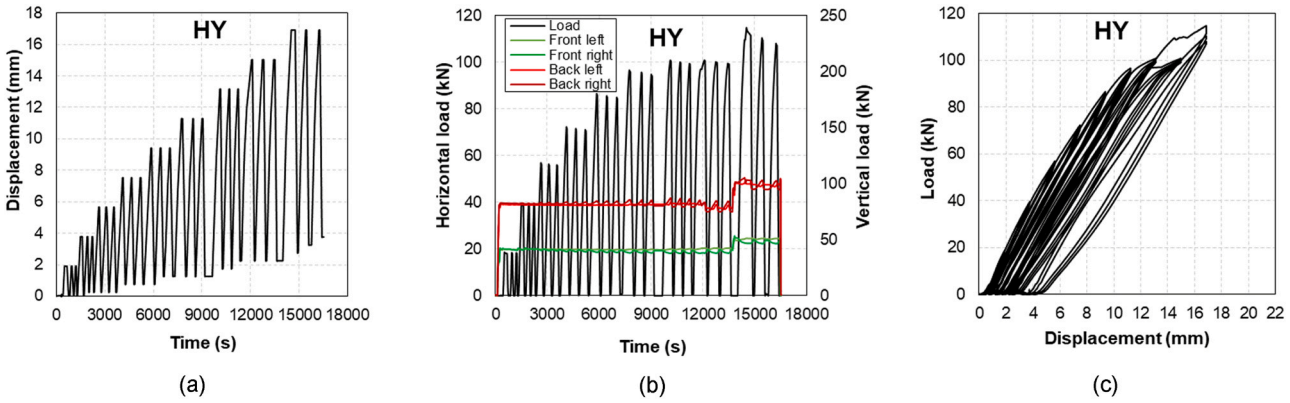

Fig. 18. (a) Horizontal (stroke) displacement-time, (b) load-time and (c) load-displacement (stroke) curves of the cyclic test with rebars and adhesive.

due to the uplift of the back walls observed during the loading phases, ranging from 153.35 kN (0.19 MPa) to 170.48 kN (0.21 MPa) in the first part of the test, and from 184.21 kN (0.23 MPa) to 205.96 kN (0.26 MPa) when the prestress load was increased.

Fig. 19 shows the crack pattern on the front wall at the end of the cyclic test with the rebars and adhesive.

Looking at the load vs displacement curves obtained from the LVDTs located on the front wall reported in Fig. 20, an increase of the displacement is evident going from the bottom to the top of the specimen. The displacements result higher (maximum of 11.9 mm) also in the middle with respect to the sides, confirming the bending mechanism already observed in the previous tests. Moreover, the right side of the wall shows higher displacements (max. 8.5 mm) with respect to the left side (max. 4.0 mm). A progressive residual displacement was also measured by all transducers. Fig. 21 shows the relative displacements measured between the front and back walls on either side (a and b, respectively), and the vertical displacement, i.e. uplift, measured on the back walls (Fig. 21c). The relative displacement is negligible on the right side, denoting an excellent connection, while on the top-left side (BL-200) a large displacement (6.14 mm) was measured where a crack developed during the monotonic test (Fig. 11b), resulting in a less effective connection. During the test, the back wall uplifted especially on the right side, reaching 4.2 mm of vertical displacement (Fig. 21c), demonstrating the effectiveness of the connection.

4. Discussion

Table 1 summarizes the main results of the performed tests in terms of maximum horizontal load, vertical load on the back walls (also in terms of actual pressure) and nominal prestress value, while Fig. 22 shows the comparison in terms of load vs displacement (stroke) curves.

A significantly different behavior can be observed between the unreinforced specimen (URM) and the specimen retrofitted using twisted bars (HE) or bonded bars (HY). The unreinforced specimen showed a higher initial stiffness with respect to both retrofitted solutions. This may be attributed to the fact that the strengthening was applied on the damaged specimen and that the cracks occurred during the monotonic test could not be completely closed (i.e. zero crack width was not recovered).

The HE specimen showed similar stiffness for the first cycles (up to 100 % of FME) with respect to the HY one. After this point, the HE specimen underwent larger displacements and a stronger loss in stiffness, associated to a high dissipation capability. Both retrofitted specimens showed a maximum load higher than the monotonic test peak load. However, for the HE solution, the monotonic peak load was reached at around 50 % larger displacement due to the stiffness degradation, while the HY specimen approximately continued (with slight parallel shift) the original curve of the URM wall (before the FME had occurred) even at displacements beyond the FME.

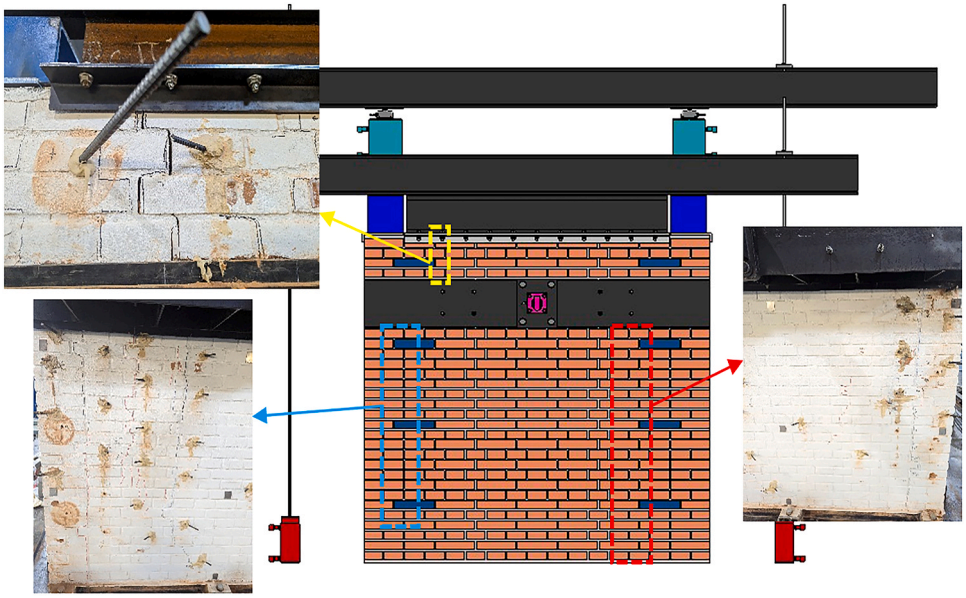

Fig. 19. Crack pattern at the end of the test with bonded rebars – front side.

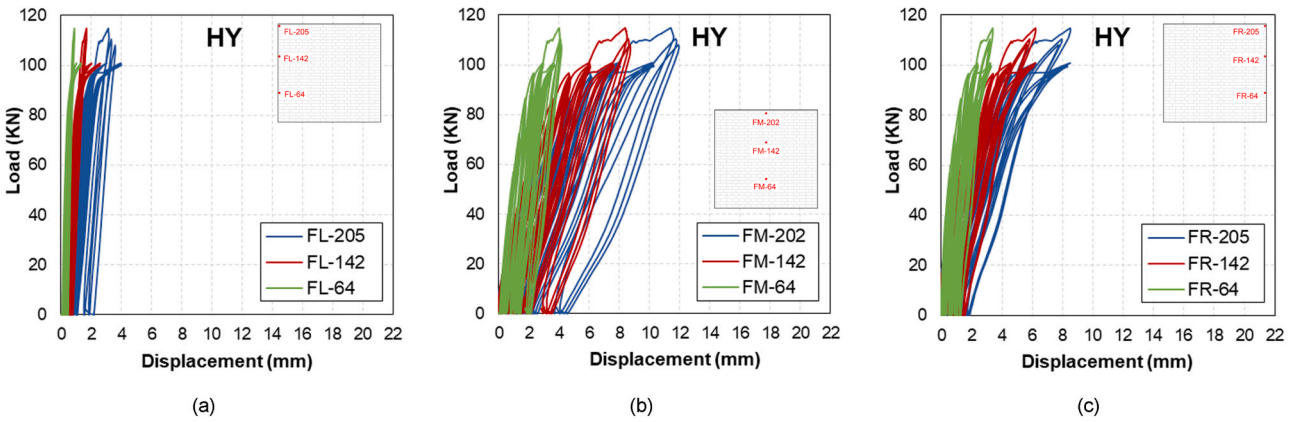

Fig. 20. Load-displacement (LVDT) curves at different height of the front wall: (a) left side, (b) middle, (c) right side.

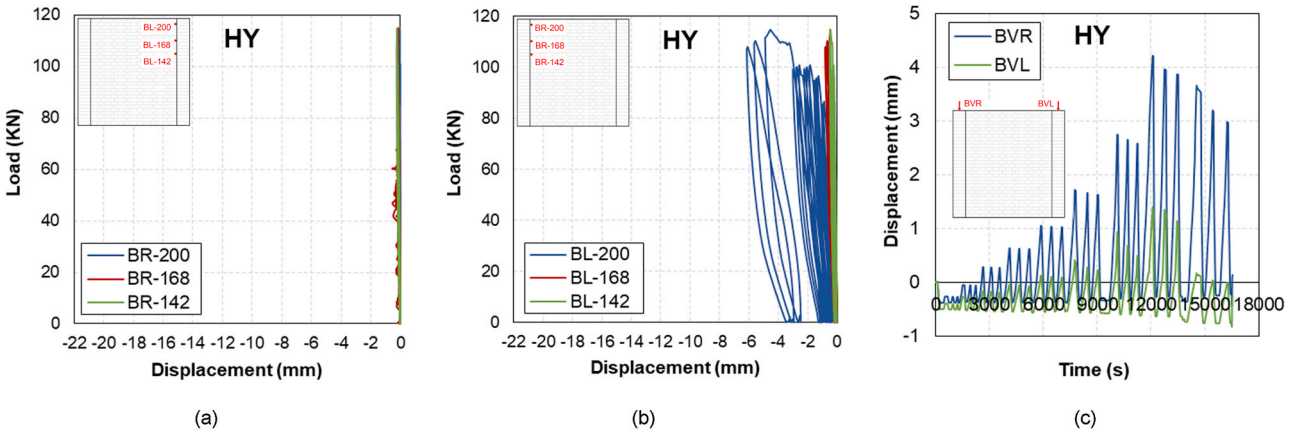

Fig. 21. Load-displacement (LVDT) curves at different height of the front wall measured from the back: (a) relative displacement on left side, (b) relative displacement on right side. In (c), vertical displacement on the back walls.

Table 1
Summary of the experimental results.

Prestress	Unreinforced			Twisted bars			Rebars +adhesive		
	Horizontal	Vertical		Horizontal	Vertical		Horizontal	Vertical	
MPa	kN	Back Left kN (MPa)	Back Right kN (MPa)	kN	Back Left kN (MPa)	Back Right kN (MPa)	kN	Back Left kN (MPa)	Back Right kN (MPa)
0.20	86.9	80.4 (0.20)	84.0 (0.21)	89.7	81.9 (0.20)	84.7 (0.21)	96.7	75.1 (0.19)	77.3 (0.19)
0.25	-	-	-	-	-	-	114.9	97.3 (0.24)	95.0 (0.24)

The drift ratio at the peak load associated to the monotonic test was 0.67 %, which increased to 1.01 % in case of the HY configuration, and to 1.23 % in case of the HE one. The values are into the limit range suggested by the Eurocode 8 [42] (0.50–1.00 %), with the exception of the HE configuration which is above the limit. However, it should be highlighted that the Eurocode range is not specifically defined for masonry structures. Considering instead the values proposed by the Italian CNR guidelines [43] for existing masonry walls failing under axial and bending, the drift ratio can range between 0.80 % and 1.20 %, in line with the experimental outcomes.

With respect to the peak load reached by the two different retrofitting solutions, it should be highlighted that the number of installed rebars with adhesive was significantly lower than the number of twisted bars (26 vs. 42). Despite this, the HY peak load resulted higher and at smaller displacements than the HE one, confirming the better performance in terms of load bearing capacity of the HY retrofitting configuration.

By increasing the external vertical prestress on the wall in the HY testing phase (from 0.20 MPa to 0.25 MPa), an increase of the horizontal bearing capacity was observed (as also observed in the previous investigation with the T-wall specimen [29]), together with a stiffness decrease.

Overall, a larger residual displacement was observed in the case of twisted bars.

Fig. 23 shows the comparison of the absolute displacement on the top of the front wall (left, middle and right). On the right side, the displacements were similar in the HE and HY configurations, with a slightly larger displacement in HE retrofitted wall. On the contrary, in the middle of the wall and on the left side, the HE retrofitted wall showed larger displacements and higher dissipation with respect to the HY one.

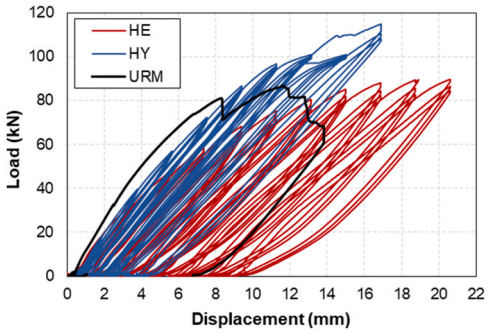

Fig. 22. Load-displacement (stroke) curves for the different tests: monotonic on the unreinforced specimen (URM), cyclic on the specimen retrofitted with twisted bars (HE) and cyclic on the specimen retrofitted with rebars and adhesive (HY).

The pre-existing cracks were stitched in both cases (with twisted bars or rebars and adhesive), but, on the basis of the experimental evidence, it can be assumed that bonded bars led to a more effective connection/repair. Nevertheless, looking at the relative displacement comparison (Fig. 24a and b), it is also evident how the stitching made with bonded bars on the left wall was not properly effective, with a maximum crack opening above 6 mm. On the right side, the relative displacement is instead negligible. The vertical uplift was more evident on the HY test (Fig. 24c), in particular on the right side, proving that a rigid motion of the specimen was activated.

Fig. 25 reports the time-displacement curves related to the top horizontal displacements measured on the front and back walls. The different cracking paths developed during the monotonic test on the left and right side of the specimen resulted in different behaviors.

On the left side, a crack developed between the front and the rear wall (Fig. 11b). In case of twisted bars, this resulted in a significant relative displacement between back and front wall (BL-200, Fig. 25a), with smaller absolute displacement associated to the back wall (BHL) in comparison to the front wall (FL-205) due to insufficient crack stitching. A better behavior was observed in case of bonded bars (Fig. 25b), where the relative displacement was limited and emerged only in the final phase of the test.

On the right side, a crack developed on the front wall (Fig. 11a). The rebars with adhesive (Fig. 25d) resulted capable to stitch the existing crack, as proved by nearly zero relative displacement (BR-200), with a perfect superposition of the absolute displacement measured at the top front wall (FR-205) and top back wall (BHR). On the contrary, considering the specimen with twisted bars (Fig. 25c), a very large relative displacement between the two walls of about 13 mm was measured (BR-200), associated to a clearly softer behavior and high dissipation. Nevertheless, since the crack was located on the front wall, coinciding displacements measured at the top front wall (FR-205) and top back wall (BHR) were recorded.

Also of high interests is the comparison of the envelope curves of the peak loads measured at the progressive cycles for the different displacement levels (Fig. 26). The load degradation between the cycles is rather limited for both twisted bars and bonded bars, with slightly higher degradations observed for the twisted bars solution, but still denoting a good cyclic behavior.

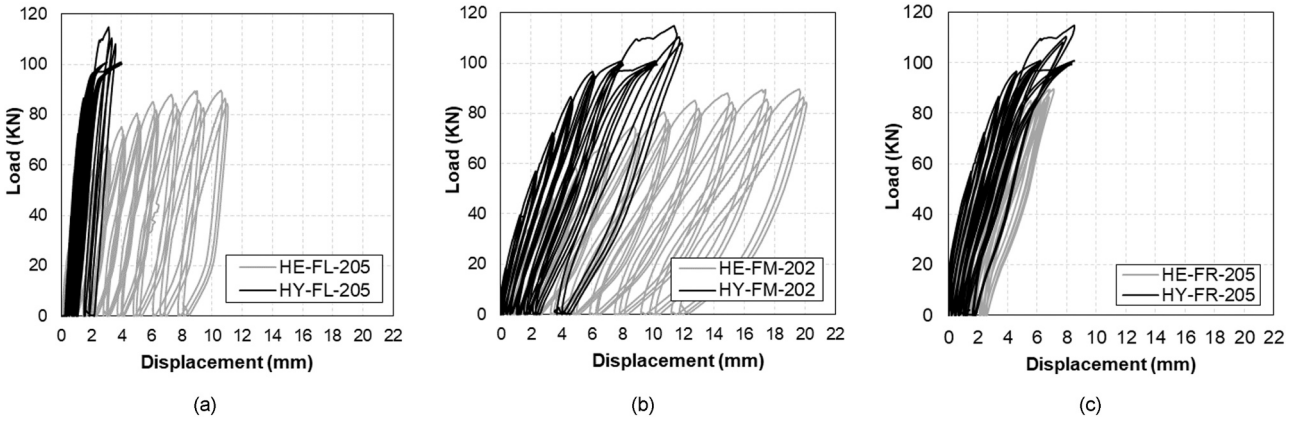

Fig. 23. Comparison of load-displacement (LVDT) curves for different strengthening techniques: (a) left side, (b) middle, (c) right side.

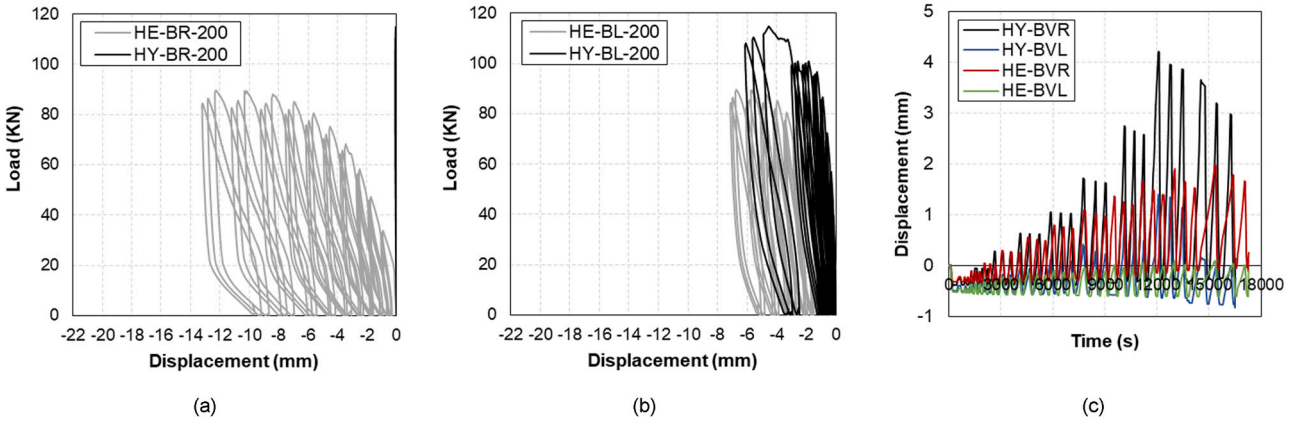

Fig. 24. Comparison of load-relative displacement (LVDT) curves for different strengthening techniques: (a) right side, (b) left side. In (c), comparison of the vertical displacement on the back walls.

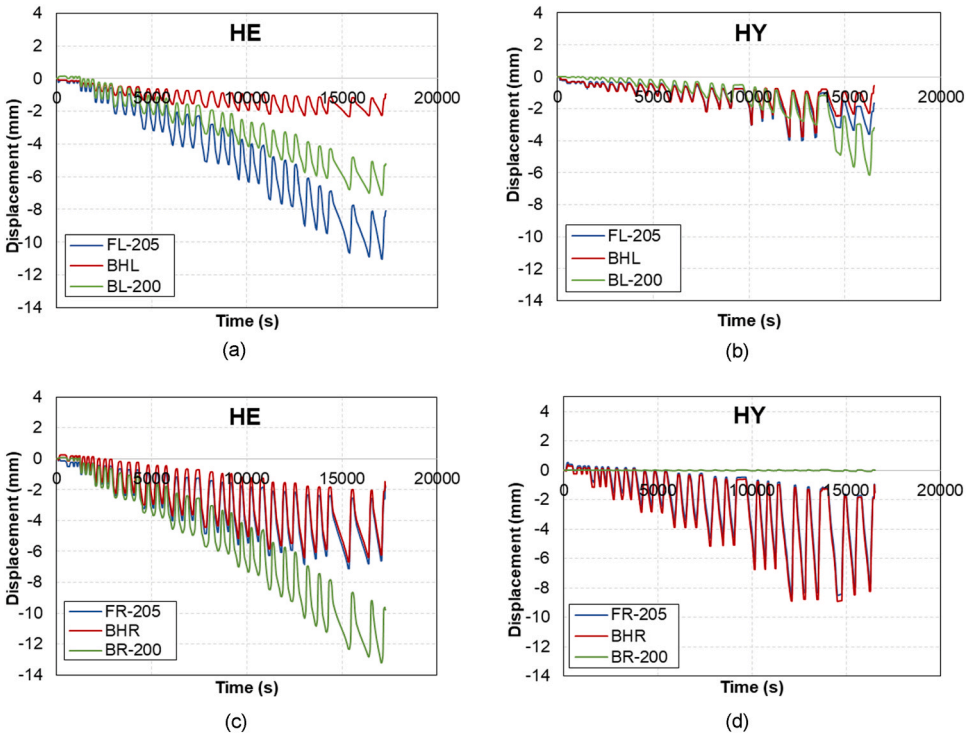

Fig. 25. Time-displacement curves at the top of the specimen for both retrofitting solutions – on the left (a-b) and right side (c-d) of the specimen.

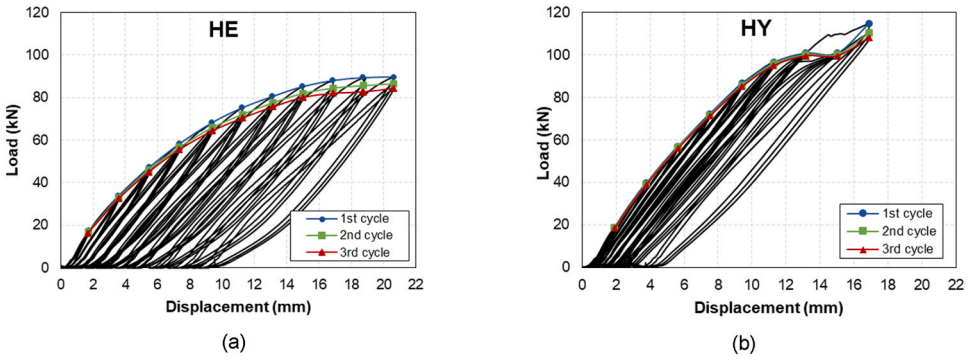

Fig. 26. Load-displacement (stroke) curves with peak loads for the different cycles for twisted bars (a) and rebars and adhesive (b).

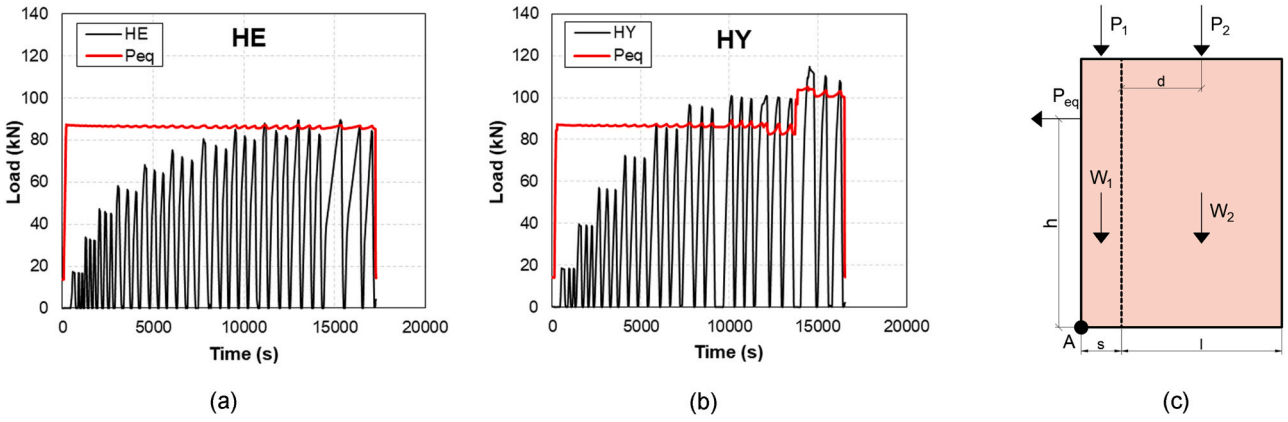

Fig. 27. Load-time curve with the evaluation of the theoretical P_{eq} for twisted bars (a) and rebars with adhesive (b). In (c), sketch of the specimen with the involved loads and lever arms.

Generally, it can be stated that the strengthening method using bonded bars seems to guarantee higher bearing capacity with a limited ductility of the connection, and the achievement of a perfect box-like behavior. On the contrary, the connection with twisted bars is characterized by lower bearing capacity and higher energy dissipation associated to large displacements.

Finally, some interesting additional considerations can be made by looking at Fig. 27, where the horizontal load vs. time curve is reported for HE and HY specimens, together with the theoretical value of the horizontal load P_{eq}, and a sketch of the specimen with the involved loads and lever arms. From experimental evidence it was noticed that, after a certain horizontal load level, by maintaining the prestress constant on the back walls, no further increase of the applied horizontal load was possible. Considering the sketch of Fig. 27c, the specimen is subjected to the external force P_{eq} as well as to the self-weight and to the weight of the steel beams, namely W_1 for the front wall (equal to 23.1 kN), W_2 for each one of the back walls (equal to 28.0 kN), and to the vertical prestress P_1 (front load) and P_2 (back load). By imposing the rocking equilibrium with respect to the point A, the Eq. (1) gives the equilibrium load P_{eq}:

$$P_{eq} = \frac{\left(W_1 + P_1\right)\cdot\frac{s}{2} + 2W_2\cdot\left(s + \frac{l}{2}\right) + P_2\cdot(s + d)}{h} \quad (1)$$

where s is the thickness of the front wall (25 cm), l is the length of the back wall (136.5 cm), d is the distance between the back of the front wall and the axis of application of the vertical prestress P_2 (equal to 68 cm), and h is the height of application of the horizontal load measured from the strong floor (167 cm).

By assuming roughly $P_1 = 84$ kN and $P_2 = 164$ kN (see Section 2.5), the theoretical equilibrium load P_{eq} results in 88 kN, while, by considering the actual loads P_1 and P_2 measured by the load cells, the results reported in Fig. 27a and Fig. 27b (red lines) are obtained for twisted bars and bonded bars, respectively.

It can be noted that both retrofitting solutions were able to reach the equilibrium load. However, in case of rebars with adhesive, the experimental horizontal load exceeded the theoretical one; indeed, a significant uplift of the specimen was observed, associated to a monolithic overturning. When the vertical prestress was increased (P1 and P2), the applied horizontal load increased as well, becoming also closer to the theoretical equilibrium value. This resulted in a reduced rotation/uplifting of the specimen.

5. Conclusions

In this paper, the experimental results of a testing program conducted on a full-scale C-shaped masonry wall subjected to out-of-plane loading have been presented and discussed. The objective was to investigate two different strengthening solutions to improve the joint connection between walls, one applying twisted steel bars in a "dry" borehole (no adhesive) and the other using bonded rebars. For this reason, the specimen has been tested considering three different configurations: (i) unreinforced, subjected to monotonic loading; (ii) retrofitted with twisted bars, subjected to cyclic loading; (iii) retrofitted with bonded bars, subjected to cyclic loading. The main findings are summarized in the following:

- both retrofitting solutions were able to recover the full capacity of the wall by re-connecting the front and the back walls; however, a different number of connectors was used in the two different cases due to the different pull-out capacities associated to the single connectors (26 rebars vs. 42 twisted bars);
- the twisted bars showed a higher dissipation capacity of the system, associated to larger displacements and higher residual displacement, with respect to the bonded rebars; on the other side, the bonded bars showed higher resistance at even lower displacements, achieving a better monolithic behavior for the specimen;
- the pre-existing crack pattern, developed during the monotonic test, influenced the performance of the retrofitted specimen, although additional bars were introduced to stitch the cracks. Indeed, the left side of the specimen was intersected by a large crack from the beginning, and even the bonded bars solution was not able to fully stitch it, allowing anyway certain displacements;
- the vertical prestress on the wall strongly affected the results of the test, and a clear change of stiffness/maximum applied horizontal load was noticed by intentionally changing its value;
- the use of adhesive with rebars seems to be the most effective solution, both in terms of load bearing capacity and monolithic behavior achieved; however, the large displacements associated to twisted bars could be a great advantage in case of earthquake actions;
- finally, it should be highlighted that twisted bars installed "dry" have the great advantage to be removable and compatible with the masonry, so their use should be preferred when dealing with historical masonry buildings.

Despite the conducted tests provided interesting results on the structural behavior of C-shaped walls retrofitted with twisted bars or bonded bars, further experimental research is needed to confirm the observed trend, considering the limited number of tested specimens. Additionally, an analytical model could be defined and validated, on the basis of the collected experimental results, for the design of wall-to-wall structural connections.

CRediT authorship contribution statement

Sara Cattaneo: Writing – review & editing, Supervision, Methodology, Investigation, Data curation, Conceptualization. **Manuela Scamardo:** Writing – review & editing, Writing – original draft, Visualization, Validation, Investigation, Formal analysis. **Navid Vafa:** Visualization, Investigation, Formal analysis. **Pietro Crespi:** Writing – review & editing, Supervision, Methodology, Formal analysis, Data curation.

Declaration of Competing Interest

The authors declare that they have no known competing financial interests or personal relationships that could have appeared to influence the work reported in this paper.

Data availability

The authors do not have permission to share data.

References

[1] E. Işık, F. Avcil, A. Büyüksaraç, R. İzol, M. Hakan Arslan, C. Aksoylu, et al., Structural damages in masonry buildings in Adıyaman during the Kahramanmaraş (Turkiye) earthquakes (Mw 7.7 and Mw 7.6) on 06 February 2023, Eng. Fail Anal. 151 (2023), https://doi.org/10.1016/j.engfailanal.2023.107405.
[2] G. Vlachakis, E. Vlachaki, P.B. Lourenço, Learning from failure: damage and failure of masonry structures, after the 2017 Lesvos earthquake (Greece), Eng. Fail Anal. 117 (2020), https://doi.org/10.1016/j.engfailanal.2020.104803.
[3] A. Penna, P. Morandi, M. Rota, C.F. Manzini, F. da Porto, G. Magenes, Performance of masonry buildings during the Emilia 2012 earthquake, Bull. Earthq. Eng. 12 (2014) 2255–2273, https://doi.org/10.1007/s10518-013-9496-6.
[4] Brandonisio G., Lucibello G., Mele E., Luca A De, De Luca A. Damage and performance evaluation of masonry churches in the 2009 L'Aquila earthquake. Eng Fail Anal 2013;34:693–714. https://doi.org/10.1016/j.engfailanal.2013.01.021.
[5] A. Furtado, H. Rodrigues, H. Varum, Simplified guidelines for retrofitting scenarios in the European countries, Energies 16 (2023), https://doi.org/10.3390/en16052408.
[6] Marques R. Masonry box behavior.,Encyclopedia of Earthquake Engineering, 2014. https://doi.org/10.1007/978-3-642-36197-5_155-1.
[7] P.B. Lourenço, N. Mendes, L.F. Ramos, D.V. Oliveira, Analysis of masonry structures without box behavior, Int. J. Archit. Herit. 5 (2011), https://doi.org/10.1080/15583058.2010.528824.

[8] G. de Felice, R. Fugger, F. Gobbin, Overturning of the façade in single-nave churches under seismic loading, Bull. Earthq. Eng. 20 (2022), https://doi.org/10.1007/s10518-021-01243-5.
[9] M.A. Elgawady, P. Lestuzzi, A review of conventional seismic retrofitting techniques for URM, 13th Int. Brick Block Mason. Conf. (2004) 1–10.
[10] S. Bhattacharya, S. Nayak, S.C. Dutta, A critical review of retrofitting methods for unreinforced masonry structures, Int. J. Disaster Risk Reduct. 7 (2014) 51–67, https://doi.org/10.1016/j.ijdrr.2013.12.004.
[11] G. Cianchino, M.G. Masciotta, C. Verazzo, G. Brando, An overview of the historical retrofitting interventions on churches in Central Italy, Appl. Sci. (Switz.) 13 (2023), https://doi.org/10.3390/app13010040.
[12] S. Podestà, L. Scandolo, Earthquakes and tie-rods: assessment, design, and ductility issues, Int. J. Archit. Herit. 13 (2019), https://doi.org/10.1080/15583058.2018.1563239.
[13] Ceroni F., Prota A. Case Study: Seismic Upgrade of a Masonry Bell Tower Using Glass Fiber-Reinforced Polymer Ties n.d. https://doi.org/10.1061/ASCECC.1943-5614.0000001.
[14] A. Maione, C. Casapulla, M. Di Ludovico, A. Prota, F. Ceroni, Efficiency of injected anchors in connecting T–shaped masonry walls: a modelling approach, Constr. Build. Mater. 301 (2021), https://doi.org/10.1016/j.conbuildmat.2021.124051.
[15] F. Ceroni, H. Darban, N. Caterino, R. Luciano, Efficiency of injected anchors in masonry elements: evaluation of pull-out strength, Constr. Build. Mater. 267 (2021), https://doi.org/10.1016/j.conbuildmat.2020.121707.
[16] A. Cascardi, M. Leone, M.A. Aiello, Transversal joining of multi-leaf masonry through different types of connector: experimental and theoretical investigation, Constr. Build. Mater. 265 (2020), https://doi.org/10.1016/J.CONBUILDMAT.2020.120733.
[17] Vintzileou E., Tselios I., Welz G., Karagiannaki D. Anchors to Masonry in Seismic Conditions: Cracked vs. Uncracked Locations, 2023. https://doi.org/10.1007/978-3-031-32511-3_29.
[18] S. Paganoni, D. D'Ayala, Testing and design procedure for corner connections of masonry heritage buildings strengthened by metallic grouted anchors, Eng. Struct. 70 (2014) 278–293, https://doi.org/10.1016/J.ENGSTRUCT.2014.03.014.
[19] G. Maddaloni, M. Di Ludovico, A. Balsamo, A. Prota, Out-of-plane experimental behaviour of T-shaped full scale masonry wall strengthened with composite connections, Compos B Eng. 93 (2016) 328–343, https://doi.org/10.1016/J.COMPOSITESB.2016.03.026.
[20] Hilti Italia S.p.A. Hilti Heli-Brick documentation and instructions for use. n.d.
[21] S. Moreira, L.F. Ramos, B. Csikai, P. Bastos, Bond behavior of twisted stainless-steel bars in mortar joints, in: Proceedings of the Ninth International Masonry Conference (2014).
[22] S. Cattaneo, M. Scamardo, Assessment of the tensile behavior of twisted steel connectors for masonry retrofitting, Constr. Build. Mater. 392 (2023), https://doi.org/10.1016/j.conbuildmat.2023.131771.
[23] C. Gentilini, F. Finelli, V.A. Girelli, E. Franzoni, Pull-out behavior of twisted steel connectors employed in masonry: the influence of the substrate, Constr. Build. Mater. 274 (2021), https://doi.org/10.1016/J.CONBUILDMAT.2020.122115.
[24] C. Gentilini, F. Finelli, C. Carloni, An experimental study of the bond behavior of twisted steel bars embedded in mortar cylinders and in the joints of masonry wallettes, Constr. Build. Mater. 316 (2022), https://doi.org/10.1016/j.conbuildmat.2021.125795.
[25] M. Corradi, A. Di Schino, A. Borri, R. Rufini, A review of the use of stainless steel for masonry repair and reinforcement, Constr. Build. Mater. 181 (2018), https://doi.org/10.1016/j.conbuildmat.2018.06.034.
[26] N. Ismail, J.M. Ingham, In-situ and laboratory based out-of-plane testing of unreinforced clay brick masonry walls strengthened using near surface mounted twisted steel bars, Constr. Build. Mater. 36 (2012), https://doi.org/10.1016/j.conbuildmat.2012.04.087.
[27] N. Ismail, R.B. Petersen, M.J. Masia, J.M. Ingham, Diagonal shear behaviour of unreinforced masonry wallettes strengthened using twisted steel bars, Constr. Build. Mater. 25 (2011), https://doi.org/10.1016/j.conbuildmat.2011.04.063.
[28] R.B. Petersen, N. Ismail, M.J. Masia, J.M. Ingham, Finite element modelling of unreinforced masonry shear wallettes strengthened using twisted steel bars, Constr. Build. Mater. 33 (2012), https://doi.org/10.1016/j.conbuildmat.2012.01.016.
[29] S. Cattaneo, P. Crespi, M. Scamardo, N. Vafa, Cyclic behavior of masonry walls retrofitted with post-installed twisted bars or bonded rebars, Constr. Build. Mater. 409 (2023), https://doi.org/10.1016/j.conbuildmat.2023.134026.
[30] F. Yavartanoo, T.H.K. Kang, Retrofitting of unreinforced masonry structures and considerations for heritage-sensitive constructions, J. Build. Eng. 49 (2022) 103993, https://doi.org/10.1016/J.JOBE.2022.103993.
[31] F.J. Baeza, L. Estevan, S. Ivorra, Seismic retrofitting of heritage structures, actual techniques and future challenges for earth and masonry constructions, RILEM Book. vol. 47 (2024), https://doi.org/10.1007/978-3-031-39603-8_87.
[32] Ministero delle infrastrutture e dei Trasporti. Decreto Ministeriale 17 Gennaio 2018 C.S.LL.PP. Aggiornamento delle «Norme tecniche per le costruzioni» 2018.
[33] Federal Emergency Management Agency, American Society of Civil Engineers. FEMA 356 Prestandard and commentary for the seismic rehabilitation of buildings, 2000.
[34] European Committee for Standardization. EN 1998-3 Eurocode 8: Design of structures for earthquake resistance - Part 3: Assessment and retrofitting of buildings Eurocode, 2005.
[35] ASTM C67/C67M-21. Standard Test Methods for Sampling and Testing Brick and Structural Clay Tile, ASTM International, 2021.
[36] ASTM C1006-13. Standard Test Method for Splitting Tensile Strength of Masonry Units, 07, 2013.
[37] C348–21. Standard Test Method for Flexural Strength of Hydraulic-Cement Mortars, Annual Book of ASTM Standards 2021;!
[38] ASTM C109/C109M-02. Standard Test Method for Compressive Strength of Hydraulic Cement Mortars, Annual Book of ASTM Standards 2020;04.
[39] BS 1881-117. Testing Concrete - Part 117: Method for Determination of Tensile Splitting Strength, British Standard Institution 1983;2.
[40] EOTA. ETA-22/0395 Injection System Hilti HIT-HY 270 in solid bricks, 2022.
[41] S. Cattaneo, N. Vafa, Tensile capacity of adhesive anchors in damaged masonry, Appl. Sci. 11 (2021), https://doi.org/10.3390/app112110135.
[42] EN 1998-1: Eurocode 8: Design of Structures for Earthquake Resistance – Part 1: General Rules, Seismic Actions and Rules for Buildings. 2004.
[43] Consiglio Nazionale delle Ricerche. CNR-DT 212/2013 - Istruzioni per la Valutazione Affidabilistica della Sicurezza Sismica di Edifici Esistenti, Roma, 2013.